

Reliability analysis of a tendon-driven actuation for soft robots

The International Journal of
Robotics Research
1–18
© The Author(s) 2020
Article reuse guidelines:
sagepub.com/journals-permissions
DOI: 10.1177/0278364920907151
journals.sagepub.com/home/ijr


Useok Jeong^{1,2*} , Keunsu Kim^{2,4*}, Sang-Hun Kim^{2,3*} ,
Hyunhee Choi⁴, Byeng Dong Youn^{2,4,5,6} and Kyu-Jin Cho^{2,3,5}

Abstract

The reliability of soft robotic devices will be the bottleneck that slows their commercialization. In particular, fatigue failure issues are a major concern. Thus, reliability should be taken into account from the earliest stages of development. However, to date, there have been no attempts to analyze the reliability of soft robotic devices in a systematic manner. When soft robots are employed to force transmission applications, reliability is typically a dominant issue, since soft robotic structures are constructed with soft material components; these materials have highly nonlinear properties that arise due to the large distribution in the material properties. Furthermore, reliability should be analyzed from the robot's system down to the components using domain knowledge about the system; this requires a systematic approach. This study presents a framework for reliability analysis of soft robotic devices taking into account a probability distribution that has not been considered before and examines a case study of a tendon-driven soft robot. This study focuses specifically on the (a) concept design process, (b) lifetime analysis process, and (c) design and optimization process. A life model that considers distribution is proposed using accelerated life testing based on analysis of the failure mechanism of the tendon-driven system. The tensile stress of the wire was varied during the experiment with different bend angles and output tension. The result was validated with different stress levels using a testbed to simulate an actual application. The proposed reliability analysis methodology could be applied to other soft robotic systems, such as pneumatic actuators, to improve the reliability-related properties during the robot design stage, and the life model can be used to estimate the device lifetime under various stress conditions.

Keywords

Tendon-driven soft robot, Bowden cable, reliability, fatigue failure, lifetime

¹Robotics R&D Group, Korea Institute of Industrial Technology (KITECH), Republic of Korea

²Soft Robotics Research Center, Republic of Korea

³Biorobotics Laboratory, School of Mechanical and Aerospace Engineering, Seoul National University, Republic of Korea

⁴Laboratory for System Health & Risk Management, School of Mechanical and Aerospace Engineering, Seoul National University, Republic of Korea

⁵Institute of Advanced Machines and Design, Seoul National University, Republic of Korea

⁶OnePredict Inc., Republic of Korea

*These authors contributed equally to this work.

Corresponding authors:

Kyu-Jin Cho, Biorobotics Laboratory, School of Mechanical and Aerospace Engineering/Soft Robotics Research Center, Seoul National University, Gwanak-ro 1, Gwanak-gu, Seoul, Korea/Institute of Advanced Machines and Design, Seoul National University, Seoul 08826, Republic of Korea.

Email: kjcho@snu.ac.kr

Byeng Dong Youn, Laboratory for System Health & Risk Management, School of Mechanical and Aerospace Engineering/Soft Robotics Research Center, Seoul National University, Gwanak-ro 1, Gwanak-gu, Seoul, Korea / Institute of Advanced Machines and Design/OnePredict Inc., Seoul National University, Gwanak-ro 1, Gwanak-gu, Seoul, Korea.

Email: bdyoun@snu.ac.kr

1. Introduction

The reliability of robotic devices is an emerging issue, especially for soft-bodied robots and robots with soft material components. The concept of soft robotics has opened up new avenues for the design of robotic devices through the use of highly adaptable soft materials, which has expanded the potential applications of the robots. Soft materials involve many nonlinearities; these are sometimes advantageous, but can also limit the capabilities of the soft robots.

Despite the many attractive advantages of soft robots, soft robotic devices are more structurally vulnerable than rigid robots and have many uncertainties in their soft structural properties (Case et al., 2015; Cianchetti et al., 2018). Although soft robotic devices have suffered from reliability issues (Godler et al., 2012; Kramer et al., 2011; Krieger et al., 2017a; Liu et al., 2018; Sun et al., 2013; Usman et al., 2017; Wang et al., 2017; Yap et al., 2015), reliability has not yet been studied systemically in the soft robotics field. In one study, a self-healing concept for soft robots was proposed (Terry et al., 2017), mimicking the healing capacities in nature to address the robot's susceptibility to damage from unpredictable environments. Soft robots are sometimes intended to be edible (Miyashita et al., 2016; Sardesai et al., 2018), biodegradable, or disposable (Miyashita et al., 2016; Walker et al., 2017). Regardless, the robots should provide reliable service during their lifetime; thus, the reliability of the soft material components is important.

Because of these problems, some studies on the fatigue life of soft robotic devices have been recently conducted to examine the life properties of the robotic devices. Durability and performance degradation of the jamming gripper were examined for the development of a commercial use soft gripper (Amend et al., 2016). Repeatability and durability of the soft pneumatic actuators were investigated with different pressures using fatigue testing (Miron and Plante, 2016; Yap et al., 2016). The lifetime of twisted string actuators in various loads, strokes with different numbers of strings (Usman et al., 2017), and materials (Godler et al., 2012) have also been studied. Wang et al. (2017) conducted a durability test of a soft gripper with different pressures and actuators. The fatigue of a flexure hinge (Krieger et al., 2017a) and origami structure (Liu et al., 2018) was also studied under different design parameters.

In spite of recent reliability studies examining soft robotic devices, the majority of studies have been limited to simple life testing and lack systematic reliability analysis tools to design the experiment and analyze and generalize the experimental results. Although the trivial regression of a lifecycle without physics context used in the previous studies is simple and intuitive for each special case, the respective testing results cannot be generalized to other cases. More importantly, previous studies have not taken into account the probability regarding uncertainties and the large property dispersion in the soft materials and robotic

structure. There exist a large number of uncertainties in soft-structure properties; these uncertainties originate from both the material itself and from the manufacturing process (Case et al., 2015). These uncertainties play an important role in the lifetime probability, as well as reliability, necessitating more statistical analysis than needed for rigid robots. Conventional design methodologies for robots have been developed to satisfy the required function and improve the performance of products. However, in practice, there exists a large gap between a product that is only function-oriented and a product that is in compliance with the reliability analysis. Thus, reliability engineering should be treated as an integral part of product development, rather than as a separate activity with little to no interaction with other development activities (Hu et al., 2018).

Generally, activities related to product reliability are categorized into five tasks that occur in three major development phases: (a) the concept phase (product reliability program, goal setting); (b) the design phase (reliability-based design, reliability testing); and (c) the production phase (production) (Hu et al., 2018). Similarly, reliability-related activities for a robotic system generally take into account the above five tasks, which consider both a system-level approach and a component-level approach. The reliability framework of a robotic device is schematically organized in Figure 1; the framework follows a top-down approach from the system level to the component level through three processes: the concept design process, the design and optimization process, and the lifetime analysis process. These processes happen during the concept phase and the design phase. Unlike the general process, this framework excludes the production phase due to limitations of demonstration at the laboratory scale. During the concept phase, a pre-investigation is accomplished to examine the target robot application to set goals related to durability, safety, cost-effectiveness, and so on. The important issues for setting the goals of reliability are determined according to the needs of users, which include failure criteria, warranty life, and cost. Once the goals have been established, potential failures for the robot application are analyzed and the failure modes of key components are selected. It is important to clearly identify failure modes and their causes, especially in soft robotic devices, because it may be ambiguous to classify failures of the soft and continuum structure. The failure modes of a tendon-driven soft robot can be reviewed based on domain knowledge of soft robotic devices; examples of failure modes include failure of the tendon actuator, the soft structure, or the tendon's routing path. Then, the target failure mode can be determined based on its criticality in the robotic application. During the design phase, the designer can satisfy the goals by reliability-based design and reliability testing. Both approaches deal with uncertainties using statistical analysis, which is based on failure distribution of the component. If component providers cannot offer failure distributions, possible choices are to use a failure database of similar parts and to estimate the distribution through

reliability testing. In many cases of new product development like soft robotic devices, the failure distribution is unknown and similar part information is hard to utilize due to the material and driving mechanisms; thus, reliability testing is needed. Reliability information (e.g., lifetime models) can be obtained by designing and performing reliability tests, such as durability tests, environmental tests, and accelerated life tests, at the design stage according to the failure mechanism that creates the specific failure mode of each component. In this case, stress is determined; stress affects the characteristics of each module and part according to the design requirements derived from the concept phase. Table 1 lists the studies regarding life testing of soft robotic devices based on the progress of the reliability analysis. The work in Table 1 determines the component that will be targeted for reliability analysis of the soft robotic devices; however, this is limited to life testing under certain conditions without a systematic framework or statistical considerations.

In this paper, the reliability analysis theories that have been conventionally used in industry are reinterpreted to apply to robotic devices to cope with the reliability issues that are prevalent in the soft robotic field today. Systematic reliability analysis of a tendon-driven soft robot is presented by adopting reliability analysis methods, including failure analysis, statistical analysis for lifetime distribution estimation, and modeling of the stress–life relation. An overview of the general framework of reliability analysis for a robot is provided. Failure modes, effects, and criticality analysis (FMECA) was performed based on a reliability-based design framework to narrow the life analysis target of the tendon-driven soft robot. Wire breakage was determined as

the targeted failure mode. As a result of this process, the lifetime distribution of the Bowden cable system in the tendon-driven soft robot can be estimated under different operating conditions.

The rest of the paper is organized as follows. The failure analysis and failure mechanism modeling of the tendon-driven soft robot is presented in Section 2. Next, in Section 3, we estimate the life model of the tendon-driven system in a soft robot using accelerated life testing (ALT) and statistical analysis. Section 4 shows validation of the life model for practical soft robot devices. Section 5 gives conclusions and suggestions for future work.

2. Failure analysis of a tendon-driven soft robot

In this research, a life model for a tendon-driven soft robot will be investigated; this can be used to estimate the lifetime of a tendon-driven soft robot under various stress levels and can be used as a design guideline for the robot, in compliance with the target lifetime. FMECA was conducted to determine the targeting failure mode based on the risk assessment of the potential failure modes. Based on the result of FMECA, breakage of the tendon was determined as an analysis target and ALT was conducted to collect the lifetime data of the tendon system under different stress conditions. Then the stress–life model of the Bowden cable is presented based on the physics of failure and statistics. Finally, the proposed life model was validated under different stress conditions to simulate the soft wearable robot and discussion about the application on general soft robotic devices is presented.

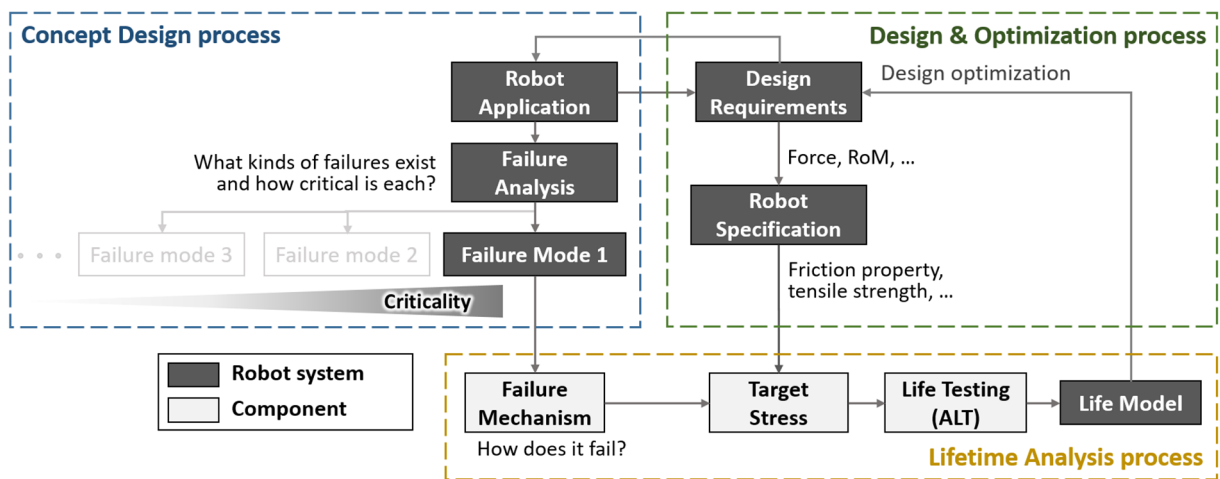


Fig. 1. The framework of reliability analysis for soft robotic devices. It mainly consists of a concept design process, a lifetime analysis process, and a design and optimization process; these are sub-categories of (a) the concept phase and (b) the design phase; two of the three major reliability-related development phases. During the concept design process, the failure modes of the system are analyzed and selected based on the reliability criteria. During the lifetime analysis process and the design and optimization process, the life model of the targeting failure mode is derived and the life model is used to estimate the lifetime at a certain stress condition and give feedback to the design process ALT: accelerated life testing.

Table 1. Comparison of framework procedures for reliability analysis.

Study	Target component	Failure analysis	Life modeling		Lifetime estimation & validation
			Statistical analysis	Stress–life relationship	
Case et al., 2015	Elastomers	△	O	X	X
Godler et al., 2012; Usman et al., 2017	Twisted spring actuators	△	X	Exponential	△
Wang et al., 2017; Yap et al., 2016	Pneumatic grippers/ actuators	△	X	X	X
Krieger et al., 2017a	Flexure hinge	△	X	Exponential	△
Liu et al., 2018	Origami structure	X	X	X	X
Miron et al., 2016	Pneumatic artificial muscles	O	X	Log-linear	X
This work	Bowden cable	O	O	Inverse power law	O

Note: This table compares the reliability analysis stages of the previous studies regarding soft robotic devices. The systematic analysis approach is required based on the reliability criteria to set up a life model that can describe and estimate the life distribution under various operating conditions.

2.1. Targeting failure mode for analysis

The reliability of the tendon-driven soft robot is affected by many factors, including failure in the actuator, damages on the soft structure, tensile stress and abrasion along the cable, etc., resulting in several failure modes, such as polymer tear, delamination cable breakage, tendon path failure, etc. However, in reality, it is inefficient and impossible to examine every potential case; therefore, it is necessary to prioritize the potential failure modes based on risk assessment by listing the potential failure modes, failure causes, failure mechanisms, occurrence, and severity. FMECA is an analytical method to systemically identify the high-priority failure modes for the target of the reliability study for a given system. It also helps enable better understanding of the failure mechanisms of a target system and gives guidance for setting up the life testing (Tumer and Stone, 2003).

Table 2 shows a FMECA worksheet for a soft robot that consists of potential failure mode, failure cause, failure mechanism, occurrence, severity, and risk for each component of the general form of a tendon-driven soft robot. The general form consists of an actuator, a force transmission (routing path in the case of tendon-driven system), and a soft structure (Figure 2). The occurrence and severity were rated considering the actual use of the tendon-driven soft robot. The risk was determined by multiplying the equally weighted occurrence and severity ratings to compare the riskiness of each failure mechanism on the system (Pecht, 2009).

Structural failure of the soft body is very common in soft robotic devices, including failure along the force transmission path (tendon routing path, air leakage in chamber, etc.), tear of the polymer, and delamination of dissimilar materials. The structural failure is caused mainly from the stress concentration due to deformation, application of the actuator, and use of dissimilar materials. For example, the tendon attachment point is very fragile, as the tendon could apply high pressure with the point or line contacts; the air pressure can induce stress concentration at a certain point

of the chamber. In addition, stress concentration occurs on the mating faces of materials that have different stiffness. However, the risk of structural failure in soft robotic devices is hard to generalize because soft robots vary in design and because the failure occurrence and severity greatly depend on the robot's specific design, material properties, interaction between dissimilar materials, manufacturing process, application, and even the competence of the manufacturing. Although structural failure sometimes causes malfunction of the robot, depending on the damaged part, these events usually have low severity, which is an advantage of soft robots. On the other hand, failure along the actuation wire has a severe effect on the actuation system of a tendon-driven soft robot. Furthermore, analysis of the failure mechanism and risk assessment for the tendon system are relatively clearer than analysis of the soft structure. As a result, the reliability analysis is narrowed to the tendon system as a way to provide an initial reliability analysis of a tendon-driven soft robot.

The risky failure modes of the tendon-driven soft robot were determined to be cable derailment inside the cable actuator and wire breakage due to the cyclic tensile loading, both receiving scores of 20. The spool-based cable actuator in the soft robotic application easily fails when the wire loses tension as the cable derails from the spool (In et al., 2017). However, since the cable derailment problem has recently been addressed through improved design of the mechanism (In et al., 2017) or via linear slider-based mechanisms (Nilsson et al., 2012; Nycz et al., 2016), wire breakage originating from the cyclic tensile loading was determined to be the most severe failure mode of a tendon-driven soft robot; thus, it was selected as an analysis target in this study. The actuation wire failure in the tendon-driven soft robot completely disables the force transmission function in the robotic system; thus, it should be avoided during the robot's entire service life. A crack arises, starting from the most severely stressed part, as cyclic loading is applied to the metal component. It eventually fails via fracture as the stress accumulates and the crack develops along the

Table 2. Failure modes, effects, and criticality analysis (FMECA) worksheet for a tendon-driven soft robot.

Element	Failure mode	Failure causes	Failure mechanism	Occurrence ^a	Severity ^b	Risk ^c		
Actuator	Cable derailment	Low tension, slack	-	4	5	20: Severe risk		
	Spool wear	Large tension, repetitive operation	Wearout	2	3	6: Moderate risk		
	Component breakage	Overloading	Fracture	1	4	4: Low risk		
Body	Force transmission (tendon routing)	Performance degradation	Motor overcurrent	Motor overheat	1	3	3: Low risk	
		Efficiency degradation	Abrasion	Wearout	5	2	10: High risk	
	Soft structure ^d	Wire breakage	Cyclic loading	Contamination	Surface roughness change due to corrosion or dust	3	2	6: Moderate risk
				Stress concentration at the tendon fixture point	Fracture	4	5	20: Severe risk
		Tendon path failure	Excessive routing curvature	Overloading	Fracture	1	5	5: Moderate risk
				Abrasion	Wearout	1	5	5: Moderate risk
		Polymer tear	Stress concentration	Contamination	Corrosion	1	5	5: Moderate risk
				Stress concentration at the tendon fixture point	Fracture	3	4	12: High risk
		Delamination of dissimilar materials	Stress concentration	Excessive routing curvature	Fracture/delamination	3	4	12: High risk
				Stress concentration	Fracture	3	3	9: Moderate risk
		Stress concentration	Fracture	3	3	9: Moderate risk		

Note: The riskiness of the failure modes can be evaluated using a FMECA worksheet to target the failure mechanism for the reliability analysis.

^aOccurrence = {5: frequent, 4: often, 3: occasional, 2: remote, 1: extremely unlikely}.

^bSeverity = {5: very high, 4: high, 3: significant, 2: low, 1: very low}.

^cRisk = Occurrence × Severity.

^dThe risk of structural failure in soft robotic devices is hard to generalize because soft robots vary in design and because failure occurrence and severity greatly depend on the robot's specific design, material properties, interaction between dissimilar materials, manufacturing process, the competence of the manufacturing, and the application.

stainless-steel cable. Although a fracture caused by cyclic loading is a common failure mechanism in the mechanical components (Dowling, 2012), cyclic loading in a tendon is distinctive since the tensile stress is induced and amplified by the frictional force along the complex routing path, thereby accelerating the crack propagation.

Abrasive damage of the inner wire could be minimized by using a stainless-steel cable with a polytetrafluoroethylene (PTFE) liner, which has a low friction coefficient (Chen et al., 2014). As stainless steel has a higher surface hardness than PTFE (Myshkin et al., 2005), the PTFE liner could delay the abrasive wearout of the stainless-steel inner wire. Other failure modes are listed in Table 2, including efficiency degradation in the inner wire and sheath liner due to abrasion and contamination, inner wire overloading, etc.

The Bowden cable, which is a continuum tendon-driven transmission, has often been integrated in soft robotic devices (Cianchetti et al., 2018; Krieger et al., 2017b; Walker, 2013). The Bowden cable has become a part of the soft robot's structure, as depicted in Figure 2, due to its compliant properties and the high degrees of freedom in its

routing path (In et al., 2015). Examples of soft robots that use Bowden-based, tendon-driven actuation include soft wearable gloves (Choi et al., 2019; In et al., 2015; Kang et al., 2016; Nilsson et al., 2012; Nycz et al., 2016; Popov et al., 2017), the Exosuit for gait assistance (Asbeck et al., 2015), upper-limb assistance devices (Chiaradia et al., 2018; Dinh et al., 2017; Park and Cho, 2017), soft manipulators (Lee et al., 2016), and soft surgical tools (Cianchetti et al., 2018; Le et al., 2016). Dissimilar to the pulley-routed tendon-driven mechanism in articulated rigid robots (Kobayashi et al., 1998; Shirafuji et al., 2014), one important issue in Bowden cable-based transmission in soft robotic devices is the high friction along the cable (Cianchetti et al., 2018; Kaneko et al., 1991; Le et al., 2016), which has a great effect on the force transmission property and greatly affects fatigue failure of the actuation system. The changing bending angle of the cable's routing path, as well as the tension of the wire, affect the friction of the cable system. The friction between the tendon and sheath results in highly fluctuating tension on the cable; this accelerates the stress fatigue accumulation. This is unlike the pulley-routed mechanism found in rigid robots, in

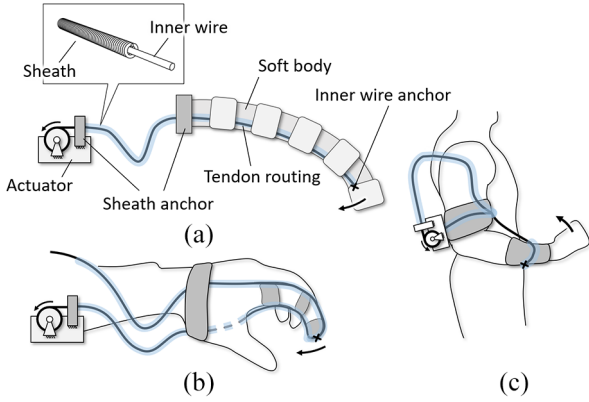


Fig. 2. Examples of tendon-driven soft robots: (a) a tendon-driven soft manipulator and (b), (c) soft wearable robots. These examples consist of an actuator, tendon routing, and soft structure. The tendon routing can be embedded inside the soft structure and routed to the actuator outside of the robot.

which fatigue of the wire is affected by the repetitive bending (Horigome and Endo, 2018). Some research has been conducted to reduce the frictional effect in the control system of a Bowden cable by using feedforward compensation (Jeong and Cho, 2015, 2017, 2019; Palli and Melchiorri, 2006) or feedback control (Asbeck et al., 2015; Kong et al., 2013; Veneman et al., 2006; Witte et al., 2015). There exists an unavoidable friction between the inner wire and the outer sheath, which enlarges the cyclic loading and accelerates the fatigue accumulation of the Bowden cable, leading to fatigue failure issues. Nevertheless, studies on the reliability of the tendon-driven system in soft robots have not been exploited and reliability remains an unsolved issue.

2.2. Modeling of the failure mechanism

The objective of the work described in this section is to derive the candidate for a life model for a Bowden cable in the tendon-driven soft robot that can estimate the probability of failure under a given operating condition. The modeling process can be divided into four steps; (a) specify the stress that affects the lifecycle; (b) derive an equivalent fatigue stress that is related to the physical quantities of the robotic application; (c) estimate the life distribution model; and (d) determine the stress–life relationship that relates the actual operating condition and the lifecycle. Figure 3 summarizes the failure mechanism analysis of the Bowden cable.

2.2.1. Background of a Bowden cable transmission. A Bowden cable consists of an inner wire to transmit the power and an outer sheath to support the inner wire’s tension and to guide the inner wire. There exists an abrasive friction between the inner wire and the outer sheath that cannot be avoided because of its transmission principle. Unlike a cable transmission that uses a pulley-bearing

system, a Bowden cable is exposed to excessive friction that increases the tensile fluctuation and eventually results in reliability issues. The tension distribution of the inner wire along the Bowden cable can be derived as follows (Kaneko et al., 1991)

$$F = \mu N \cdot \text{sgn}(v) \quad (1)$$

$$dT = F \quad (2)$$

where v is the velocity of the wire relative to the sheath, N is the normal force between the wire and the sheath, T is the wire’s tension, and F is the axial force applied to the wire segment in Figure 4. The force equilibrium between the normal force (N) and the tension (T) can be represented as shown in (3) if wire segment ($d\phi$) is sufficiently small

$$N = T \sin(d\phi) \approx Td\phi \quad (3)$$

The tension distribution along the cable can be derived from (1)–(3), resulting in the Capstan equation (Kaneko et al., 1991)

$$T(p) = \begin{cases} T_{in} \exp[-\mu\phi \cdot \delta] & (p < L_1) \\ T_0 & (L_1 \leq p) \end{cases} \quad (4)$$

$$L_1 = \min\{p \in T(p) = T_0\} \quad (5)$$

$$T_{in} = T(p=0) \quad (6)$$

$$T_{out} = T(p=L) \quad (7)$$

where $T(p)$ is the tension of the wire at position p ; μ is the coefficient of kinetic friction between the sheath and the wire; ϕ is the summation of the bent angle of each segment, $d\phi$; v is the velocity of the wire relative to the sheath; L_1 is a minimum position, p , along the wire at which $T(p) = T_0$; and L is the total length of the sheath. The tension distribution along the cable illustrates that the input–output force transmission efficiency is exponentially related to the accumulated bending angle along the cable. In addition, there exists a nonlinear hysteresis, that is, dead zone, that causes the transient change of input tension between $T_{out} \cdot \exp(\mu\phi)$ and $T_{out} \cdot \exp(-\mu\phi)$, depending on the moving direction of the cable, although a consistent output tension is applied. This transient input tension change acts as a cyclic loading and induces tensile stress leading to fatigue failure of the inner wire.

2.2.2. Deriving an equivalent fatigue stress. Although the fatigue stress on the inner wire is accumulated along the entire routing path, the wire will break at the most vulnerable part of the routing path. In the work described in this section, the most stressful part of the routing path was analyzed using the mean stress effect correction.

The mean stress effect has been known to have a major effect on the crack process-related stress–life fatigue of the materials; this can be modeled with the mean and amplitude of the cyclic stress (Zhu et al., 2017). One commonly adopted mean stress correction model for ductile material

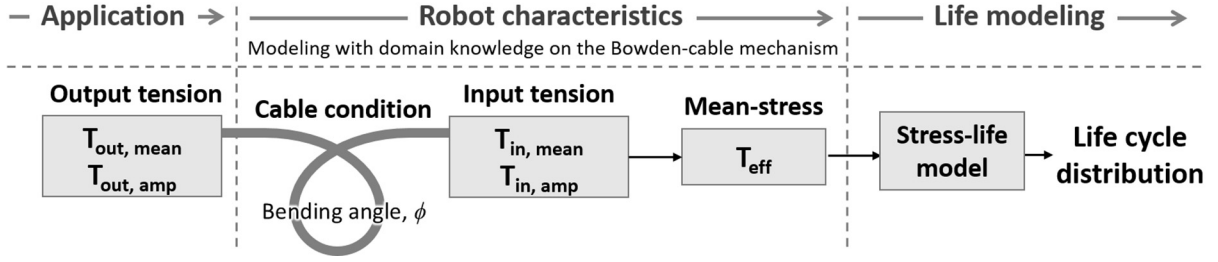


Fig. 3. A summary of failure analysis for a Bowden cable in a soft robotic device. The objective of this procedure is to define the fatigue life-related stress and to relate the stress level to the operating condition. In the case of a Bowden cable, it was found that the input tension is directly related to the fatigue life and it was also related to the operating condition (output tension and bending angle of the cable) based on the Bowden cable's friction model.

(i.e., stainless-steel wire) is the Gerber model (Bannantine et al., 1990; Wehner and Fatemi, 1991), which is represented as

$$\sigma_{ar} = \frac{\sigma_a}{1 - (\sigma_m/\sigma_u)^2} \quad (8)$$

where σ_{ar} is an equivalent stress that causes the same fatigue life under the load cycle with the stress amplitude, σ_a , and mean stress, σ_m , and σ_u is the ultimate tensile strength. The fatigue life-related equivalent stress in this model is linearly proportional to the stress amplitude without offset. This means that the zero tensile amplitude does not affect the fatigue life (e.g., a wire with free weight hanging will not break over time if there is no cyclic stress). In addition, a denominator of (8) implies that the ratio of mean stress to ultimate tensile strength multiplies the equivalent stress. Here, the stress, σ , can be substituted with the tension, T , under the assumption of the nonchanging cross-sectional area of the cable.

The equivalent tension along the entire wire, $T_{ar}(p=x)|_{\{0 \leq x \leq L\}}$, can be calculated from the desired output tension, T_{outs} , of the Bowden cable with the output tension's mean and amplitude, $T_{out,m}$ and $T_{out,a}$, specifically

$$T_{ar}(p=x)|_{\{0 \leq x \leq L\}} = \frac{T_a(x)}{1 - (T_m(x)/T_u)^2} \quad (9)$$

From the Capstan formula in (4)–(7), the equivalent tension can be proven to have a maximum value when $x=0$ for $\{\phi \geq 0\}$ and $\{T_{out} \geq 0\}$ under the condition of a passive external environment and a constant curvature along the cable. This is valid for the changing T_{out} and ϕ regardless of the sequence and the simultaneity; examples include the cases of changing ϕ in the continuum manipulator and the hand as it bends (Figures 2(a) and (b)) with an arbitrary T_{out} and changing T_{out} with fixed ϕ in an upper-arm wearable device (Figure 2(c)). This results in the fatigue life effective equivalent tension (which will be nominated as effective tension) T_{eff}

$$T_{eff} \equiv T_{ar}(p=0) = \max \left\{ T_{ar}(p=x) \Big|_{\{0 \leq x \leq L\}} \right\} \quad (10)$$

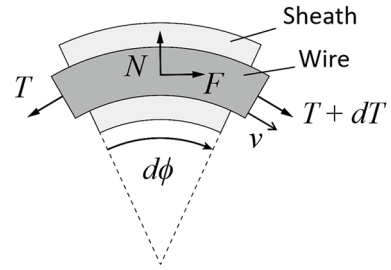


Fig. 4. Schematic diagram of a static friction model along a Bowden cable.

That is to say, the equivalent tension at the input port ($p=0$) of the cable is always largest along the routing path and, as a result, the wire fracture will develop first at the input part of the routing path. This is also supported by the experimental result—every wire specimen was broken at the input part. Therefore, the input tension, not the tension distribution, is directly related to the fatigue life.

The fatigue life effective equivalent tension, T_{eff} , can be calculated from the output tension ($T_{out,m}$ and $T_{out,a}$) using given application requirements and (4)–(7), (9)–(10), as below

$$T_{eff} = \frac{T_{in,a}}{1 - (T_{in,m}/T_u)^2} \quad (11)$$

$$T_{in,m} = \left(\frac{\eta^{-1} + \eta}{2} \right) \cdot T_{out,m} + \left(\frac{\eta^{-1} - \eta}{2} \right) \cdot T_{out,a} \quad (12)$$

$$T_{in,a} = \left(\frac{\eta^{-1} - \eta}{2} \right) \cdot T_{out,m} + \left(\frac{\eta^{-1} + \eta}{2} \right) \cdot T_{out,a} \quad (13)$$

$$\eta = \frac{T_{out}}{T_{in}} = \exp(-\mu\phi) \quad (14)$$

where η is the input–output efficiency of the Bowden cable transmission derived from (4) ranging from 0 to 1. The effective tension is proportional to $T_{out,a}$ and $T_{out,m}$ and inversely proportional to the efficiency, as illustrated in Figure 5. The interesting part in Figure 5 is that the effective tension converges to zero as the efficiency gets close to 1 when $T_{out,a} = 0$. This implies that the tensile stress will not exist if there is no tension amplitude on the wire. On

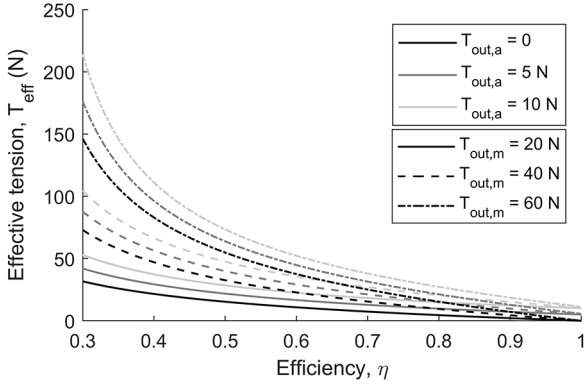


Fig. 5. Effect of the efficiency, $T_{out,a}$ and $T_{out,m}$ change on the effective tension. The effective tension is proportional to the $T_{out,a}$ and $T_{out,m}$ and is inversely proportional to the efficiency. This graph also shows that the equivalent tension increases with the bending angle of the cable system because the bending angle is inversely proportional to the efficiency, as shown in (14).

the other hand, although $T_{out,a}$ is zero, the effective tension increases as the efficiency decreases, that is, as the Bowden cable bends. Figure 5 also explains (10) that T_{ar} is largest at the input port since the efficiency along the cable can be considered to decrease with the cable's position in the bent cable. It is obvious from (12) and (13) that the input tension ($T_{in,m}$ and $T_{in,a}$) converges to the output tension ($T_{out,m}$ and $T_{out,a}$) respectively) as the efficiency (η) increases. The above equations imply that the fatigue life effective equivalent tension (T_{eff}) is a function of the output tension ($T_{out,m}$ and $T_{out,a}$) and the bending angle (ϕ). Therefore, the fatigue life of the Bowden cable can be estimated from the robot's force requirement and operating condition.

3. Experiments and model fitting

In the work described in this section, statistical analysis on the lifecycle of the cable was performed to derive the life model of the Bowden cable system for a given operating condition. The derived life model in this section could be used as a guideline for maintenance of the cable system or as a model to estimate the designed lifetime under various operating conditions. As a first step, ALT of the Bowden cable was designed and carried out to analyze the life distribution of the cable under varying application conditions; specifically, the cable's bending angle and output tension. The accelerated life test is a life testing protocol (Hu et al., 2018) that accelerates the targeting failure mechanism, to efficiently and economically collect data and derive the life model. The ALT experiment is designed to provide a larger stress than the actual operating condition to speed up the test while preserving the targeting failure mechanism.

3.1. Accelerated life testing

ALT exposes a product to the harsher working conditions to stimulate the failure faster than in actual conditions. ALT is

a formal process for measuring and improving the reliability of a product in an appropriate and cost-effective manner (Hu et al., 2018).

ALT shortens the time to failure by applying external stress to the product that is greater than that in the actual use condition. If too much stress is applied during the test, a failure that does not appear in actual use may occur due to another failure mechanism. Therefore, three conditions must be satisfied within the stress range:

- 1) consistency of failure mechanism;
- 2) the existence of a speed decision stage;
- 3) $T_d = AF \times T_a$ (T_d : actual condition life, T_a : acceleration condition life, AF : acceleration factor).

3.2. Experimental setup

An experimental setup was designed to count the lifecycles and measure the input tension of the Bowden cable with different bending angles to simulate the various operating conditions and change the friction along the cable while exerting the force to the wire. The setup mainly consists of four parts; a direct current (DC) motor with a crank-like mechanism, a tension measurement system, a cable specimen, and a weight. The DC motor (Dynamixel H54-200-S500-R, Robotis) with a linkage of length of 25 mm connected with a wire, creates a rotational motion at a constant speed of 20 RPM. A crank and pulley mechanism generates the sinusoidal reciprocating motion of the wire through the sheath. The experimental setup is assumed to only deal with the pulling force of the cable; this assumption is based on the general use of a flexible-strand cable in a soft robotic application. The load cell (333FDX, Ktoyo) is located between the pulley and the cable specimen to measure the input tension of the Bowden cable. The cable specimen consists of stainless-steel wire (uncoated, 0.457 mm diameter with 7×19 strands, SAVA cable) that has low-hysteresis, high-fatigue, and flexible characteristics with an ultimate tensile strength (T_u) of 177.4 N. The dimension of the cable is determined considering the flexibility of the cable and the general applications of tendon-driven soft robots, in which the tension on the wire does not typically exceed 100 N (Chiaradia et al., 2018; Jeong and Cho, 2017). The PTFE inner liner (1.5 mm \times 2.0 mm diameter, Myungsung FEC, Korea) and a spring sheath (2.2 mm \times 3.0 mm diameter, stainless steel, custom-made from Hanguk-cheongwon, Korea) rolls over the three-dimensional (3D) printed cable support to maintain the bending angle and support the normal forces applied on the sheath. The friction coefficient between the PTFE inner liner and the stainless-steel wire was calculated to be 0.128 by averaging the initial friction coefficient of each experimental result. A weight of 5 kg is connected to the output of the cable specimen to provide a constant load on the Bowden cable during the experiment. The room temperature was kept at 23–27°C to minimize the thermal effect on the materials. Data was collected using a data acquisition

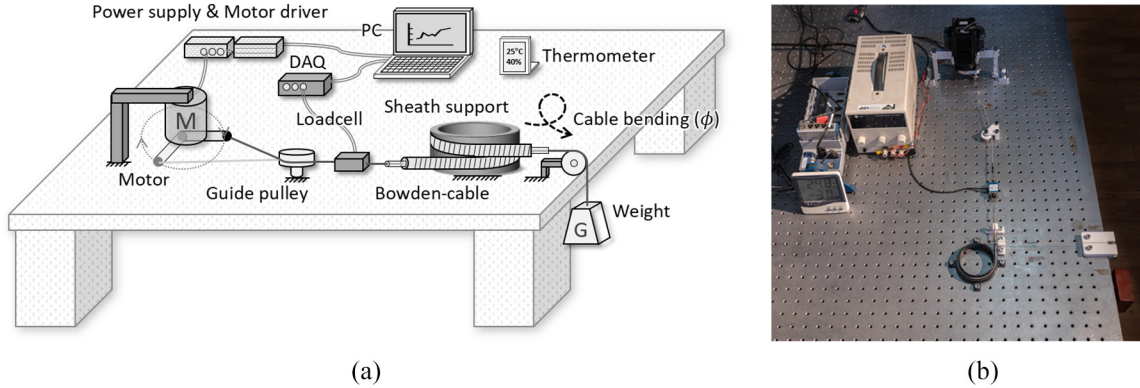


Fig. 6. The experimental setup consists of a motor-crank mechanism, tension measurement system, cable specimen, and weight. Figure (b) shows the experimental setup with a bending angle of 270° . DAQ: data acquisition.

(DAQ) system (cDAQ-9172 with NI-9237, National Instrument) with a sampling frequency of 1.6×10^3 Hz. The experimental setup described above is illustrated in Figure 6.

3.3. Experimental design

Among the main stress conditions of failure are the cable's bending angle and the applied load, as outlined in (11)–(14). The bending angle was selected as the operational factor of the ALT. Since the tension of the cable shows an exponential relationship according to the bending angle, varying the bending angle easily generates a significant difference of the lifecycle.

The ALT of the Bowden cable was conducted by varying the bending angle of the cable specimen under harsher conditions than normal operating conditions. The ranges of effective tension and bending angles were set to be similar to or larger than those observed in actual use conditions, while satisfying the consistency of the failure mechanism of ALT, as discussed in Section 3.1. The actual in-use stress condition of the soft wearable glove (In et al., 2015) and the upper-arm wearable robot (Chiaradia et al., 2018) can be calculated to be $T_{eff} \approx 25.5$ N ($T_{in,m} \approx 25.0$ N and $T_{in,a} \approx 25.0$ N with $\phi \approx 360^\circ$) and 39.9 N (the upper-arm is assumed to be lifted from 15° to 150° of the elbow joint), respectively, according to Equations (11)–(14). The experimental condition of T_{eff} was determined to range from 42.5 to 99.4 N, with bending angles of 315° , 360° , 405° , 450° , and 540° , avoiding excessive bending angles that involve unexpected nonlinearities. Twenty-two sets of experiments were performed for each condition; this number of experiments is sufficient for estimation of lifetime, which follows a Weibull distribution (Gope, 2002). The testing conditions were designed not to exceed the ultimate tensile strength of the cable. In addition, the same experiment with 270° was conducted as well to validate the proposed model. Input tension of the cable and the lifecycles until failure were

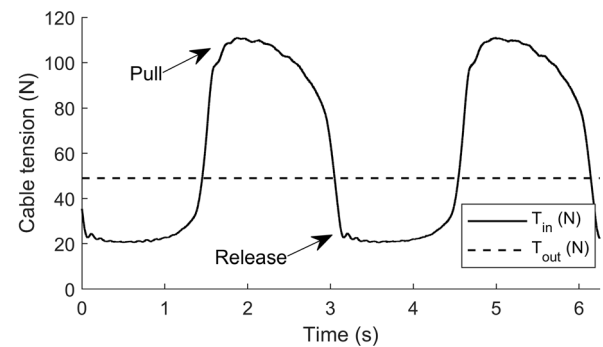


Fig. 7. The measured input tension (T_{in}) during the experiment while pulling and releasing the cable. The dashed line and dash-dotted line represent the output tension (T_{out}) and effective tension (T_{eff}), respectively.

measured until wire breakaway. The measured input tension was used to determine the friction coefficient of the specimen cable and to observe the cable breakdown. Curvature of the cable bending, total cable length, and temperature of the experimental setup were controlled to be similar for each set of trials. The end-point of the inner sheath and the outer sheath were strictly fixed to restrict the relative movement that causes decrement of the cable lifetime. Among the 22 sets of experimental data for each condition, two sets showing maximum and minimum lifecycles were excluded to screen the outliers and obtain a more statistically robust dataset (Brown and Forsythe, 1974). Figure 7 shows the input tension of the cable during the experiment, which included pulling and releasing the cable with constant output tension applied. The fluctuating input tension represents the amplified tensile stress that originated from the friction along the cable, as described in Section 3. The cyclic loading on the input port of the cable, which is the greatest along the wire, causes the wire to break at the input port with the fatigue life effective equivalent tension illustrated as a dash-dotted line in Figure 7.

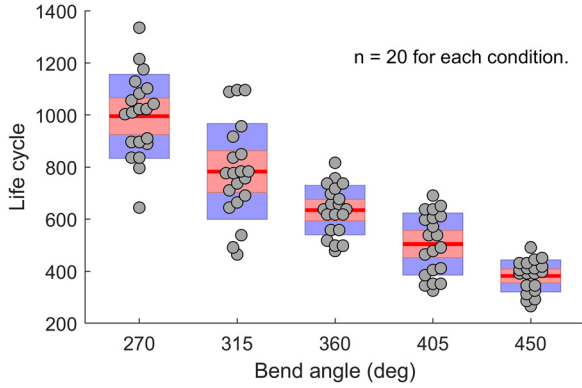


Fig. 8. Accelerated life testing results showing the lifecycle of the Bowden cable in different conditions of bending angle, 315°, 360°, 405°, and 450° with the validation set of 270°, while applying 49.0 N output tension ($n = 20$ for each condition).

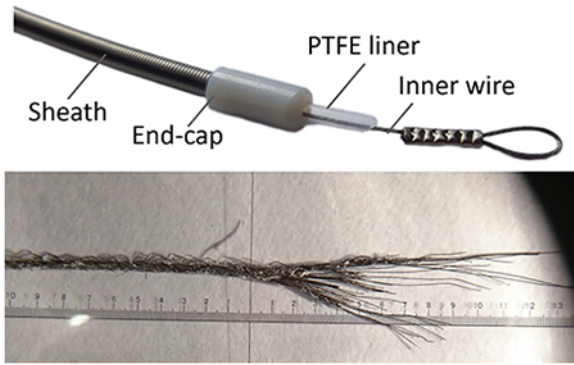


Fig. 9. The specimen consists of an inner wire, a polytetrafluoroethylene (PTFE) liner, a sheath, and an end-cap (a). The inner wire breaks at the input port of the cable system where the friction amplified tensile stress is largest (b).

3.4. Results

Figure 8 shows the ALT results, showing cycles at failure of the Bowden cable for four different bending angles, together with the validation sets at 270°. The experimental data with 540° was dismissed since it does not show an acceptable distribution, as compared to the other data. This is discussed in more detail in Section 3.5.3. It is evident that the lifecycles have some distribution and would be expressed with a certain probability density function. An appropriate distribution function that describes the results will be proposed and verified in the next section. Meanwhile, Figure 9 shows where the cable is broken near the input port of the Bowden cable, which was predicted to fail in the failure analysis section. Every trial of the experiment was terminated with the cable breakdown at the input port of the cable, as predicted in the previous section.

Table 3. Goodness of fit test for each acceleration stress distribution.

Bending angle	Type	P -value	
		K-S GoF	A-D GoF
270°	Normal	0.896	0.996
	Lognormal	0.694	0.977
	Weibull	0.955	0.978
315°	Normal	0.715	0.884
	Lognormal	0.966	0.883
	Weibull	0.581	0.792
360°	Normal	0.851	0.970
	Lognormal	0.645	0.906
	Weibull	0.981	0.977
405°	Normal	0.818	0.743
	Lognormal	0.732	0.655
	Weibull	0.735	0.731
450°	Normal	0.286	0.751
	Lognormal	0.173	0.578
	Weibull	0.517	0.888

K-S GoF: Kolmogorov–Smirnov goodness of fit; A-D GoF: Anderson–Darling goodness of fit.

3.5. Lifetime model for a Bowden cable

In this section, a lifetime model was constructed using statistical analysis on the ALT result. Firstly, cycles of life for each stress level were fitted to the lifetime distribution. To select the best-fitting distribution, the goodness of fit test was performed. With the chosen distribution, common statistical parameters were estimated for overall data that could represent a targeting failure behavior. Lastly, the stress–life relationship was revealed based on experimental results and understanding of physics of failure.

3.5.1. Fitting of the lifetime distribution. For most fatigue failures, the lifetime often follows a specific distribution depending on the stress level and the failure mechanism (Hu et al., 2018; Jung et al., 2016; Kim et al., 2017). Table 3 shows a comparison of the goodness of fit test result for normal, lognormal, and Weibull distributions under each bending condition. The Weibull distribution showed the best result, with an average P -value for Kolmogorov–Smirnov goodness of fit (K-S GoF) of 0.754 and Anderson–Darling goodness of fit (A-D GoF) of 0.873 against the normal distribution (0.713, 0.869) and the lognormal distribution (0.642, 0.869). Although the normal or lognormal distributions were well-fit in several cases, the Weibull distribution could represent the whole data with knowledge of the failure mechanism; the Weibull distribution has been widely used to represent the fatigue failure distribution by cyclic loading for electronic and mechanical parts (Hu et al., 2018; Jung et al., 2016; Kim et al., 2017).

Table 4. Weibull-distribution parameters.

Bending angle	Effective tension, T_{eff} (N)	Scale parameter, α	Shape parameter, β
270°	35.1	1.06×10^3	6.94
315°	42.5	8.54×10^2	4.79
360°	50.7	6.75×10^2	7.70
405°	60.0	5.51×10^2	5.09
450°	70.8	4.07×10^2	7.64
^a 540°	99.4	2.36×10^2	3.34

^aThe experimental data with 540° was dismissed for the life modeling since the shape parameter of the 540° case ($\beta_{540^\circ} = 3.34$) was shown to be far below the shape parameter of other cases. It is considered that the condition of 540° involves too much stress on the system, resulting in a different failure mechanism.

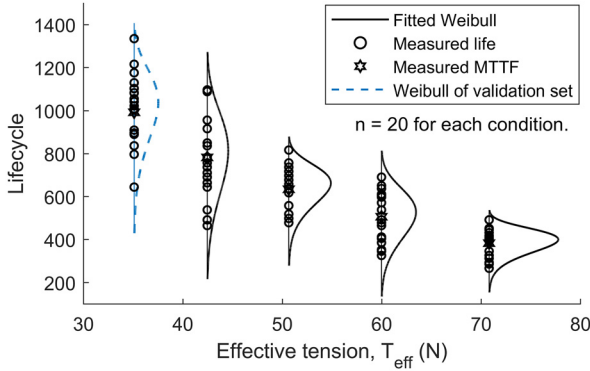


Fig. 10. The fitted Weibull distribution of lifecycles for each stress level, including the validation set of 270° ($n = 20$ for each condition). The stars are the mean time to failure (MTTF) for each dataset [993, 783, 634, 506, 383].

The Weibull probability density function can be expressed with the shape parameter (β) and the scale parameter (α), which describe Weibull slope and distribution respectively

$$f(x|\alpha, \beta) = \frac{\beta}{\alpha} \left(\frac{x}{\alpha}\right)^{\beta-1} e^{-(x/\alpha)^\beta} \quad (15)$$

Here, the shape parameter (β) is related to the failure mechanism; it should be within a certain range regardless of the stress level for the same type of failure mechanism. The scale parameter (α), on the other hand, is inversely related to the level of stress—fatigue life effective equivalent tension, T_{eff} in (11)—for a given lifetime distribution. The effective tension, T_{eff} , for each experiment condition was calculated using (11) with $\{T_u = 177.4 \text{ N}; T_{out,m} = 49.0 \text{ N}; T_{out,a} = 0\}$. The scale parameter and shape parameter of the Weibull distribution under each bending angle were calculated using maximum likelihood estimation (MLE); these are listed in Table 4. The experimental data with 540° was dismissed for the life modeling since the shape parameter of the 540° case ($\beta_{540^\circ} = 3.34$) was shown to be far below the shape parameter of other cases and because it does not satisfy the consistency condition of ALT, as discussed in Section 3.1. It is considered that the condition of 540° involves too much stress on the system,

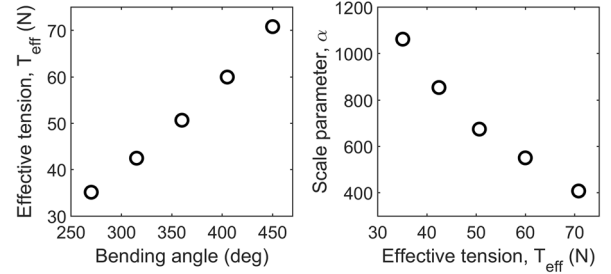


Fig. 11. The relationship between the bending angle, effective tension, and scale parameter. The effective tension increases with the bending angle as the amount of friction increases. The fitted Weibull scale parameter is inversely related to the effective tension.

resulting in a different failure mechanism. Figure 10 illustrates the fitted Weibull for each experimental condition showing the lifetime distribution at the effective tension. Figure 10 shows that the data variance decreases as the stress level increases, because the influence of the main stress on the life span becomes dominant and the deviation decreases. However, in the case of the effective tension of 60.0 N, it shows a different tendency. Here, it is assumed that other factors affect the results, since the shape parameter value is slightly different from the other case. Therefore, the shape parameters of each experimental condition were determined to be between 4.79 and 7.70, which is a tolerable range that describes the same type of failure mechanism (Ban and Anusavice, 1990).

Figure 11 compares the parameters related to the stress level: the bending angle, effective tension, and scale parameter. It is shown that the effective tension is proportional to the bending angle and that the scale parameter of the Weibull distribution shows an inversely proportional relationship in a logarithmic scale with the effective tension, as expected. The estimated stress–life relationship with regard to the distribution and its validation will be presented in the next section.

3.5.2. Estimation and verification of the common shape parameter. The objective of life modeling is to estimate the probability density function at a given stress level based

on the ALT results that were analyzed in the previous section. It can be assumed that there exists a common shape parameter (McCool, 2012) representing several Weibull populations, fitted in Table 4, to make a representative distribution model. Then, the estimation of the common shape parameter, $\hat{\beta}$, can be calculated with the MLE by solving the equation below (Nelson, 2009; Yang and Lin, 2007)

$$\sum_{i=1}^k r_i \left(\frac{\sum_{j=1}^{n_i} t_{ij}^{\hat{\beta}} \log t_{ij}}{\sum_{j=1}^{n_i} t_{ij}^{\hat{\beta}}} \right) - \frac{\sum_{i=1}^k r_i}{\hat{\beta}} - \sum_{i=1}^k \sum_{j \in D_i} \log t_{ij} = 0 \quad (16)$$

where $t_{ij}(j = 1, \dots, n_i)$ are the lifetimes and censoring times in the sample from the i th Weibull population ($i = 1, \dots, k$), r_i is the number of measured lifetimes in the i th sample, and D_i is the set of individuals in the measured i th sample. The common shape parameter, $\hat{\beta}$, was determined to be 5.94; this will be used as a delegate shape parameter of the Weibull distribution for the Bowden cable in this study. To quantitatively verify the assumption that the estimated common parameter represents an identical failure mechanism, a likelihood-ratio test (Kim et al., 2017) should be performed. The null hypothesis is that Weibull distributions at different J stress levels have a common shape parameter ($\hat{\beta}$)

$$H_0 : \beta_1 = \beta_2 = \dots = \beta_J = \hat{\beta} \quad (17)$$

The alternative hypothesis (H_1) is that shape parameters at different stress levels are not the same. The function of test statistics (Λ) is defined as

$$\Lambda = 2 \log L(\hat{\alpha}_1, \dots, \hat{\alpha}_J, \hat{\beta}_1, \dots, \hat{\beta}_J) - 2 \log L(\hat{\alpha}_1, \dots, \hat{\alpha}_J, \hat{\beta}) \approx \chi^2(1 - \alpha_s; J - 1) \quad (18)$$

where $L(\cdot)$ is the likelihood function and $\chi^2(\cdot)$ is the chi-square distribution with a significance level α_s . The distribution of Λ follows a chi-square distribution with $J - 1$ degrees of freedom (J : degree of freedom (DOF) of the alternative hypothesis; 1: DOF of the null hypothesis). If Λ is equal to or less than $\chi^2(1 - \alpha_s; J - 1)$, H_0 is accepted, where $\chi^2(1 - \alpha_s; J - 1)$ is the 100(1 - α_s) percentile of the chi-square distribution with $J - 1$ degrees of freedom. Using the results in Table 4, Λ is calculated to be $3.16 < \chi^2(0.95; 3) = 7.82$; thus, it was determined that the estimation is acceptable.

3.5.3. Stress–life relationship. The work described in the previous section estimated the common shape parameter to determine the Weibull parameters that will be used in the estimated life model. This section, then, will estimate the scale parameter for a given stress level from the Weibull distribution of the experimental results. The life distribution at a certain stress level can be represented by the probability density function, that is, Weibull distribution in this work, and the parameters of the probability density

function can be related with the stress level. In this section, the scale parameter representing the stress level will be related to the inverse power model to derive the life model in consideration of the life distribution.

The relationship between lifetimes at various levels of stress depends on the sort of stresses—such as mechanical loading, vibration, electrical voltage, current, humidity, and temperature difference—in the accelerated life test as well as the actual application. One widely used stress–life relationship—examples are for the bearings and bolts—regarding the crack propagation due to cyclic mechanical fatigue is an inverse power law (IPL) (Hu et al., 2018), which is adopted as a candidate stress–life model in this section. Specifically

$$IPL(V) = \frac{A}{(V)^\gamma} \quad (19)$$

where $IPL(V)$ represents the lifecycle-related parameter at the stress level V , and A and γ are the parameters determined by the properties of the material, the failure mechanism, and the testing method. In the Bowden cable's failure mode with the cyclic tensile stress, the lifetime–stress relationship is assumed to be represented by the inverse power model as the fatigue failure is caused by the mechanical loading.

The life distribution in (15) can be combined with the stress–life relation in (19) by substituting α with $IPL(V)$ to derive an IPL-Weibull model resulting in the desired life model with the probability considered

$$\begin{aligned} f(x) &= \left(\frac{\hat{\beta}}{\alpha} \right) \left(\frac{x}{\alpha} \right)^{\hat{\beta}-1} e^{-\left(\frac{x}{\alpha}\right)^{\hat{\beta}}} \\ &= \left(\frac{\hat{\beta}}{A/V^\gamma} \right) \left(\frac{x}{A/V^\gamma} \right)^{\hat{\beta}-1} e^{-\left(\frac{x}{A/V^\gamma}\right)^{\hat{\beta}}} \end{aligned} \quad (20)$$

3.5.4. Validation of the proposed model. Figure 12 illustrates the estimated stress–life relationship and its distribution that are fitted to (20) from the experimental results of 315°, 360°, 405°, and 450°, excluding 270° as a validation set, which result in $A = 1.53 \times 10^5$ and $\gamma = 1.38$ with a fitting root mean square error (RMSE) of 12.3. The validation set of 270° ($T_{eff} = 35.1$ N) is also plotted in Figure 12(a) showing the coincidence with the estimated lifecycle distribution and the mean time to failure (MTTF). The MTTF (Choi et al., 2018) can be used for quantitative comparison

$$MTTF|_{Weibull} = \alpha \cdot \int_0^\infty e^{-x} x^{1/\beta} dx \quad (21)$$

The MTTF at the validation condition was estimated and measured to be 1044 and 993, respectively, with a RMSE of 5.1%, which is a satisfactory result.

The B10 life, a measure of the lifecycle by which 10% of a product will have failed, can be calculated from the

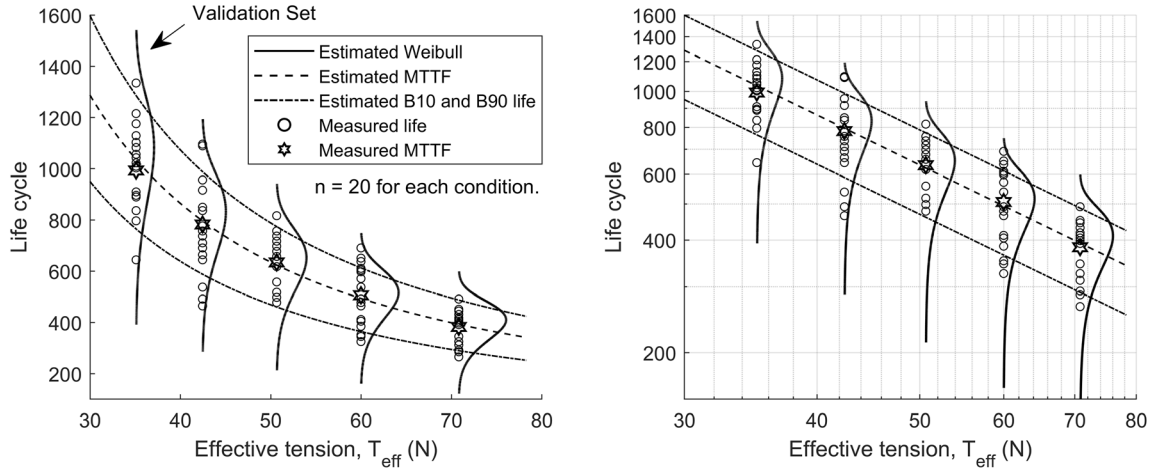


Fig. 12. The estimated stress–life relation with the Inverse power model and the validation data (a). Linearity of the stress–life relation is found clearly in a logarithmic scale (b). The solid lines and dashed line indicate the estimated distribution and mean time to failure (MTTF), respectively. The dash-dotted lines are the estimated B10 and B90 lives, respectively. The data in (a) are the measured validation data, comparing how the estimated distribution is matched with the validation data ($n = 20$ for each condition). The MTTF of the validation set showed 993 cycles, which is 5.1% smaller than the estimated cycles of 1.04×10^3 .

lower cumulative distribution of the Weibull (15), which is commonly used as a lifetime criteria for a product

$$P(B_x|\alpha, \hat{\beta}) = \int_0^{B_x} f(t|\alpha, \hat{\beta}) dt = 1 - e^{-(B_x/\alpha)^{\hat{\beta}}} = x\% \quad (22)$$

where P is the cumulative probability of Weibull and B_x is the $B_x\%$ life at which $x\%$ of the product will have failed. The B10 and B90 lives are illustrated in Figure 12 with the dash-dotted lines. It can be seen that 2 and 19 data points out of 20 data of the validation set are within the range of B10 and B90. The data in Figure 12(a) are the measured validation data, comparing how the estimated distribution is matched with the validation data. It appears that the estimated distribution is well-matched graphically in the probability plot (Nelson, 2009) with the MTTF error of 5.1 % (estimated: 1.04×10^3 cycles; measured: 993 cycles).

3.5.5. Summary. This section presented a life model of a Bowden cable using the life distribution and the stress–life relationship. (a) The ALT was designed and conducted to measure the lifecycle for the various stress levels by changing the bending angle of the cable. (b) The life distribution was able to be described by the Weibull distribution and the representative distribution was presented with the common shape parameter, $\hat{\beta}$. (c) The stress–life relationship was presented by relating the scale parameter of the Weibull with the stress level using the inverse power model. (d) The probability considered life model was derived as a result by combining the Weibull and inverse power model, which was (e) validated with the data at 270° .

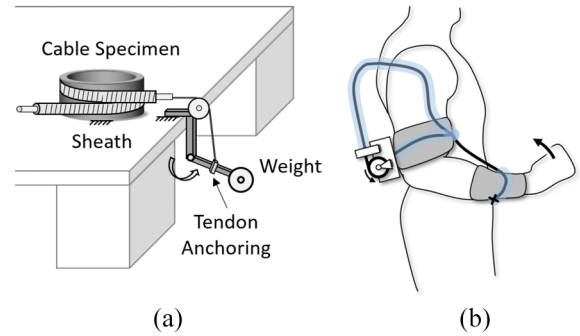


Fig. 13. A simulated testbed of an actual application (a) of a tendon-driven soft robot with a 1-degree-of-freedom upper-arm actuation (b). A sinusoidal tension is applied to the output port of the cable as the moment arm of the cable on the joint changes.

4. Application for a tendon-driven soft robot

In this section, an actual application simulated testbed with varying tension depending on the stroke of the cable was designed to further verify the life model proposed in the previous section. The life testing and the life modeling of the Bowden cable was performed under constant output load in the previous section, while changing the bend angle to vary the fatigue-related stress, that is, T_{eff} . The fatigue effective tension, T_{eff} , depends not only on the bend angle but also on the output tension, as derived in (11). In practical applications of a soft wearable robotic device, the output tension applied to the actuating cable changes depending on the kinetics of the robot system or the contact stiffness when grasping an object, such as in the case of a wearable robot for the ankle, the upper arm, or the hand (Chiaradia et al., 2018; In et al., 2015; Nycz et al., 2016; Park and Cho, 2017).

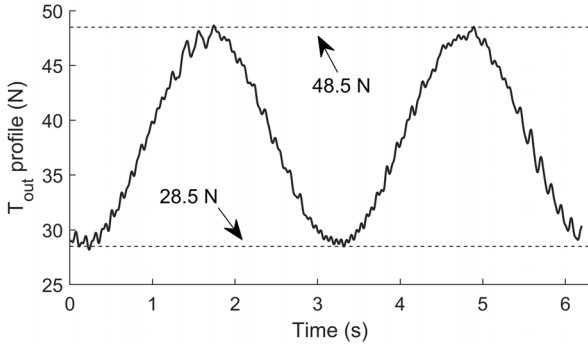
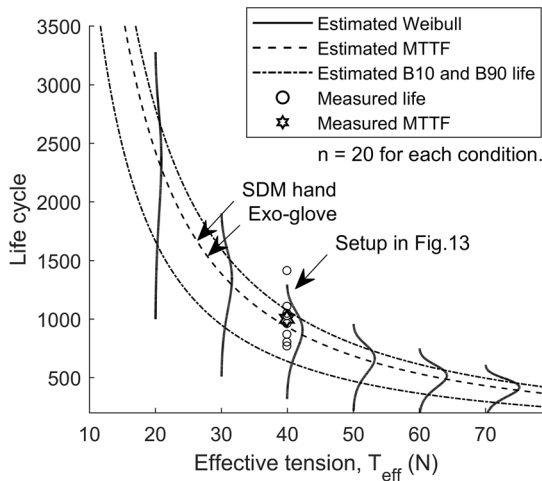


Fig. 14. The load profile simulating the soft wearable robotic application, acting as T_{out} in the experimental setup. The tension was measured without the sheath to eliminate the frictional effect and capture T_{out} . T_{eff} was calculated to be 39.9 N from (11).

The experimental setup was designed as shown in Figure 13 to simulate the varying load conditions of a 1-dof tendon-driven soft robotic device for the upper arm in Figure 2. The same experimental setup described in the previous section was used and the 5 kg weight was substituted to the upper-arm to mimic linkages with a weight of 1.2 kg. The Bowden cable was anchored on the end-effector to actuate the rotational joint. The sinusoidal output tension (T_{out}) was applied to the setup with the periodic stroke of the cable with the minimum and maximum tension of 28.5 and 48.5 N, respectively. Figure 14 shows T_{out} that was measured without the sheath to dismiss the effect of friction and purely measure T_{out} . The bending angle of the sheath was fixed to 270° considering the ordinary design of the upper-arm soft wearable robot (Chiaradia et al., 2018; Park and Cho, 2017). Among the 12 sets of experimental data with each condition, two sets showing maximum and minimum lifecycles were excluded to screen the outliers.



4.1. Result

The effective tension, T_{eff} , was calculated to be 39.9 N from the condition above, with $T_{out,a} = 10.0$ N, $T_{out,m} = 38.5$ N, and $\phi = 270^\circ$. Figure 15 shows the estimated life model derived in the previous section depicted in the solid for the estimated Weibull, dashed line for the estimated MTTF, and the dash-dotted line for the estimated B10 and B90 lives, respectively. The eight samples of measured lifetime indicated with circles are within the range between B10 and B90 lives, and two samples are observed to be out of the range of B90 life. The MTTF was calculated to check how well the life model estimates the mean lifetime of the soft wearable robotic application. The MTTF of the soft robotic application was recorded to be 1.00×10^3 cycles; this is 13.6% longer than the estimated MTTF = 867 cycles, which is a reasonable range taking the experimental condition change into consideration.

4.2. Application examples

4.2.1. Input tension constraint. A tendon-driven soft wearable robotic hand robot, the Exo-glove (In et al., 2015), generates 0–50 N input tension from the motor, resulting in a grasping force of around 20 N at a sheath bending angle of 90° and a routing angle of 270° . In this case, regardless of the grasping force and the bending angle, only the input tension (T_{in}) affects T_{eff} , as discussed in Section 2.2.2. Thus, T_{eff} is calculated to be 25.5 N from (11); $T_{in,m} = 25.0$ N and $T_{in,a} = 25.0$ N. The B10 life, MTTF, and B90 life are estimated to be 1.19×10^3 , 1.74×10^3 , and 2.00×10^3 cycles, respectively, according to the estimated stress–life relation shown in Figure 15.

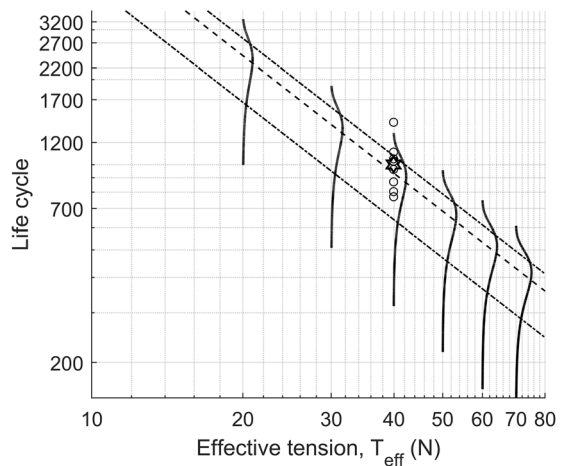


Fig. 15. Comparison between the estimated model (solid lines; Weibull distribution, dashed line: mean time to failure (MTTF) curve, dash-dotted lines: B10 and B90 life curves) and the experimental results on $T_{eff} = 39.9$ N of the simulated tendon-driven soft robot application with 10 samples (a) and in a logarithmic scale (b). The MTTF of the experimental data was recorded to be 1.00×10^3 cycles, which showed a 13.6% larger result compared to the estimated MTTF = 867 cycles. The estimated MTTF for the Exo-glove and SDM Hand applications are 1.74×10^3 and 1.79×10^3 cycles, respectively.

4.2.2. Output tension constraint. For the compliant grasper with flexure joints, the SDM Hand, the required output tension (T_{out}) is estimated to be 28 N to actuate one flexure joint (Odhner and Dollar, 2012). The input tension, $T_{in,m}$ and $T_{in,a}$, can be calculated from Equations (12) and (13), with the initial cable bending angle of the SDM Hand, $45^\circ + 25^\circ = 70^\circ$, and with the range of motion of 90° for two joints, $\eta \approx \exp\{-\mu(70^\circ + 90^\circ \times 2)\}$. This results in $T_{in,m} \approx 24.5$ N, $T_{in,a} \approx 24.5$ N, and $T_{eff} \approx 25.0$ N from (11). The B10 life, MTTF, and B90 life are estimated to be 1.22×10^3 , 1.79×10^3 , and 2.06×10^3 cycles, respectively, from the stress–life relation in Figure 15.

4.3. Discussion

The reliability of soft robots has been a dominant issue and currently bottlenecks their release into the commercial market (Amend et al., 2016); while this is the case, this issue has still to be studied in a systematic manner. Thus, this study is of significance because it employs a statistical approach to the reliability analysis of soft robots, a necessity for the future commercial use of these devices. Not only does it provide a design guideline for manufacturers, but it also provides a guideline for the lifecycle of the devices or components that will ultimately be sold to customers; the B10 life index is useful for measuring the life expectancy of a given product. In addition, this reliability analysis framework can be extended to other soft robotic systems, such as pneumatic actuators, by adopting the mechanical models and properties that are generally used for those systems to analyze their failure mechanisms and find their stress–life relationship. The reliability analysis of soft robotic systems cannot be performed only by researchers who study reliability theory, since domain knowledge on targeting systems is crucial when determining FMECA and the stress factors of these systems. For example, with pneumatic actuated robots (Miron and Plante, 2016; Sun et al., 2013; Yap et al., 2015), FMECA can be derived using a similar format to that in Table 2, but it demands inside knowledge of the manufacturing process and its application-based structural design in order to categorize failure modes and determine their occurrence and severity. In addition, the kinematics and kinetics of the PneuNet will play an important role in developing the relationship between its design parameters (size of the chamber, the thickness of walls, pressure, range of motion, etc.) and its fatigue-related stress factors (illustrated for the tendon system in Figure 3).

Especially with the experimental results in this paper, the derived life model and the parameters can be directly applied to a targeted system if it shares the same cable properties used in this study’s experiment. An example of estimating the lifecycle with varying output tension was reviewed in Section 4; the same process can be applied to other conditions. A designer can estimate the reliability properties of the cable system—including the probability density function, MTTF, B10 life, and so on—for various

operating conditions before conducting time-consuming experiments in practice. There could be a feedback loop between the reliability assessment and the design optimization during the design of the robot to improve the reliability of the system. Besides the design optimization, a developer could also predict the possible reliability-related issues in the final product from the model, while developing the prototype. Further, in terms of reliable design, measured lifetime should be embraced through use of an estimated lifetime distribution and representative quantities of measured lifetime distribution should be less than those estimated for a conservative design. If the cable properties that do not have a direct relation with the model parameter change, however, it is unavoidable that additional data will be needed to supplement the proposed model parameters in this study. Nevertheless, the shape parameter of the Weibull distribution should be within the range of the value derived in this study, and the subsequent studies with different cable properties will make a base from which to step forward toward a more generalized model.

Defining the exact operating conditions of a real-world application is not a trivial problem; thus, conditions were simplified for the experiment setup in this study. Although the stress conditions tested in this study are the constant effective tensions for each experiment, the stress condition in an actual application would consist of several stress levels. This makes the direct use of the life estimation method difficult. In that case, cumulative damage models can be adopted to determine the cumulative damage of the different stress levels on the system. One of the simplest models is Miner’s rule (Bannantine et al., 1990), which represents life consumption through a linear combination of the stress level and the proportion of repetition. As a simple example, the representative effective tension for a condition consisting of two effective tensions, 40 and 50 N, with equal operating proportion can be calculated as the condition only subjected to the effective tension of 44.34 N by solving $IPL(x) = 0.5 \cdot IPL(T_{eff} = 40\text{N}) + 0.5 \cdot IPL(T_{eff} = 50\text{N})$. In addition, the experiments in this study were conducted in an extremely controlled laboratory environment. However, in real-world applications there will exist many unexpected influencing factors, including changes of temperature and humidity, dust, and so on, that will increase the error of life-cycle estimation, demanding the use of a safety factor.

5. Conclusion

The inherent uncertainties in the properties of the soft material and deviations during the manufacturing process in soft robots, unlike rigid robots, require new reliability-related design guidelines and criteria. This study proposed a stepping stone for examining the reliability of soft robotic devices. The proposed framework adopted reliability analysis theories that have been conventionally used in industry for decades. The reliability of components used in rigid robots has been verified by industry for decades through accumulated

databases outlining reliability criteria. Unfortunately, newly emerging soft robotic components lack experience and empirical data. In addition, soft robots that are deficient in modularization, unlike the rigid robots, require a comprehensive reliability consideration from the beginning of the design process to provide a system-level perspective.

This study examined reliability analysis of a tendon-driven soft robot, starting from the system level to determine the analysis target that is the riskiest to the system. Then, the analysis scope was narrowed down to specify the origin of the fatigue stress, and this specified fatigue stress was related to the lifecycle and the operating condition of the robot using domain knowledge of the robotic system. Validation was pursued by examining the experimental condition and the robot simulated condition; validation showed satisfactory results estimating the lifecycle of the cable system for a given operating condition. In addition, reliability analysis of other soft robots, particularly tendon-driven soft robots, shows the possibility that the proposed framework can be applied to the overall soft robotics field. Nevertheless, a reliability study on a soft robot cannot be done by an individual study: it requires numerous case studies, experiences, and data accumulation. Thus, this problem will require further study and participation of the robotic society.

Acknowledgements

Useok Jeong, Keunsu Kim, and Sang-Hun Kim contributed equally to this work. The authors would like to thank Sooho Kim and Hyejeong Son in the Seoul National University Laboratory for System Health & Risk Management for the advice on statistic processing.

Declaration of conflicting interests

The author(s) declared no potential conflicts of interest with respect to the research, authorship and/or publication of this article.

Funding

The authors disclosed receipt of the following financial support for the research, authorship, and/or publication of this article: This work was supported by a National Research Foundation of Korea (NRF) grant funded by the Korean Government (MSIP) (2016R1A5A1938472), the convergence technology development program for the bionic arm through the National Research Foundation of Korea funded by the Ministry of Science and ICT (2015M3C1B2052817), the Korea Institute of Industrial Technology under “Development of Soft Robotics Technology for Human-Robot Coexistence Care Robots” (KITECH EO190021), and the Basic Research Lab Program through the National Research Foundation of Korea (NRF) grant funded by the Ministry of Science and ICT (2018R1A4A1059976).

ORCID iDs

Useok Jeong  <https://orcid.org/0000-0001-9856-2711>

Sang-Hun Kim  <https://orcid.org/0000-0003-0971-9292>

References

- Amend J, Cheng N, Fakhouri S, et al. (2016) Soft robotics commercialization: Jamming grippers from research to product. *Soft Robotics* 3(4): 213–222.
- Asbeck AT, De Rossi SMM, Holt KG, et al. (2015) A biologically inspired soft exosuit for walking assistance. *The International Journal of Robotics Research* 34(6): 744–762.
- Ban S and Anusavice KJ (1990) Influence of test method on failure stress of brittle dental materials. *Journal of Dental Research* 69(12): 1791–1799.
- Bannantine JA, Comer JJ and Handrock JL (1990) *Fundamentals of Metal Fatigue Analysis*. New Jersey: Prentice Hall.
- Brown MB and Forsythe AB (1974) Robust tests for the equality of variances. *Journal of the American Statistical Association* 69(346): 364–367.
- Case JC, White EL and Kramer RK (2015) Soft material characterization for robotic applications. *Soft Robotics* 2(2): 80–87.
- Chen D, Yun Y and Deshpande AD (2014) Experimental characterization of Bowden cable friction. In: Xi N and Hamel B (eds) *2014 IEEE international conference on robotics and automation (ICRA)*, Hong Kong, 31 May–5 June 2014, pp. 5927–5933. New York: IEEE.
- Chiaradia D, Xiloyannis M, Antuvan CW, et al. (2018) Design and embedded control of a soft elbow exosuit. In: Laschi C and Iida F (eds) *2018 IEEE international conference on soft robotics (RoboSoft)*, Livorno, Italy, 24–28 April 2018, pp.565–571. New York: IEEE.
- Choi H, Kang BB, Jung B-K, et al. (2019) Exo-Wrist: A soft tendon-driven wrist-wearable robot with active anchor for dart-throwing motion in hemiplegic patients. *IEEE Robotics and Automation Letters* 4(4): 4499–4506.
- Choi W, Youn BD, Oh H, et al. (2018) A Bayesian approach for a damage growth model using sporadically measured and heterogeneous on-site data from a steam turbine. *Reliability Engineering & System Safety*. 184: 137–150.
- Cianchetti M, Laschi C, Menciassi A, et al. (2018) Biomedical applications of soft robotics. *Nature Reviews Materials* 3(6): 143–153.
- Dinh BK, Xiloyannis M, Cappello L, et al. (2017) Adaptive backlash compensation in upper limb soft wearable exoskeletons. *Robotics and Autonomous Systems* 92: 173–186.
- Dowling NE (2012) *Mechanical Behavior of Materials: Engineering Methods for Deformation, Fracture, and Fatigue*. 4th ed. Boston: Pearson.
- Godler I, Sonoda T and Sakurai K (2012) Modeling and evaluation of a twist drive actuator for soft robotics. *Advanced Robotics* 26(7): 765–783.
- Gope PC (2002) Determination of minimum number of specimens in S-N testing. *Journal of Engineering Materials and Technology* 124(4): 421–427.
- Horigome A and Endo G (2018) Investigation of repetitive bending durability of synthetic fiber ropes. *IEEE Robotics and Automation Letters* 3(3): 1779–1786.
- Hu C, Youn BD and Wang P (2018) *Engineering Design under Uncertainty and Health Prognostics*. New York: Springer.
- In H, Jeong U, Lee H, et al. (2017) A novel slack-enabling tendon drive that improves efficiency, size, and safety in soft wearable robots. *IEEE/ASME Transactions on Mechatronics* 22(1): 59–70.

- In H, Kang BB, Sin M, et al. (2015) Exo-Glove: A wearable robot for the hand with a soft tendon routing system. *IEEE Robotics Automation Magazine* 22(1): 97–105.
- Jeong U and Cho K-J (2015) Feedforward friction compensation of Bowden-cable transmission via loop routing. In: Zhang J and Knoll A (eds) *2015 IEEE/RSJ international conference on intelligent robots and systems (IROS)*, Hamburg, Germany, 28 September–3 October, pp.5948–5953. New York: IEEE.
- Jeong U and Cho K-J (2017) A feasibility study on tension control of Bowden-cable based on a dual-wire scheme. In: Chen I-M and Nakamura Y (eds) *2017 IEEE international conference on robotics and automation (ICRA)*, May 2017, pp.3690–3695. New York: IEEE.
- Jeong U and Cho K-J (2019) Control of a Bowden-cable actuation system with embedded BoASensor for soft wearable robots. *IEEE Transactions on Industrial Electronics*. 8 October 2019. DOI: 10.1109/TIE.2019.2945212.
- Jung BC, Yoon H, Oh H, et al. (2016) Hierarchical model calibration for designing piezoelectric energy harvester in the presence of variability in material properties and geometry. *Structural and Multidisciplinary Optimization* 53(1): 161–173.
- Kaneko M, Yamashita T and Tanie K (1991) Basic considerations on transmission characteristics for tendon drive robots. In: *fifth international conference on advanced robotics*, Pisa, Italy, 19–22 June 1991, pp.827–832, New York: IEEE.
- Kang BB, Lee H, In H, et al. (2016) Development of a polymer-based tendon-driven wearable robotic hand. In: Kragic D, Bichi A and De Luca A (eds) *2016 IEEE international conference on robotics and automation (ICRA)*, Stockholm, Sweden, 16–21 May 2016, pp.3750–3755. New York: IEEE.
- Kim DW, Oh H, Youn BD, et al. (2017) Bivariate lifetime model for organic light-emitting diodes. *IEEE Transactions on Industrial Electronics* 64(3): 2325–2334.
- Kobayashi H, Hyodo K and Ogane D (1998) On tendon-driven robotic mechanisms with redundant tendons. *The International Journal of Robotics Research*. 17: 561–571.
- Kong K, Bae J and Tomizuka M (2013) Torque mode control of a cable-driven actuating system by sensor fusion. *Journal of Dynamic Systems, Measurement, and Control* 135(3): 031003.
- Kramer RK, Majidi C, Sahai R, et al. (2011) Soft curvature sensors for joint angle proprioception. In: Khatib O and Sukhatme G (eds) *2011 IEEE/RSJ international conference on intelligent robots and systems*, San Francisco, USA, 25–30 September 2011, pp.1919–1926, New York: IEEE.
- Krieger YS, Kuball CM, Rumschoettel D, et al. (2017a) Fatigue strength of laser sintered flexure hinge structures for soft robotic applications. In: Zhang H and Vaughan R (eds) *2017 IEEE/RSJ international conference on intelligent robots and systems (IROS)*, Vancouver, Canada, 24–28 September 2017, pp.1230–1235. New York: IEEE.
- Krieger YS, Roppenecker DB, Kuru I, et al. (2017b) Multi-arm snake-like robot. In: Chen I-M and Nakamura Y (eds) *2017 IEEE international conference on robotics and automation (ICRA)*, Singapore, 29 May–2 June 2017, pp.2490–2495. New York: IEEE.
- Le HM, Do TN and Phee SJ (2016) A survey on actuators-driven surgical robots. *Sensors and Actuators A: Physical* 247: 323–354.
- Lee J-Y, Kang BB, Lee D-Y, et al. (2016) Development of a Multi-functional Soft Robot (SNUMAX) and performance in RoboSoft Grand Challenge. *Frontiers in Robotics and AI* 3.
- Liu T, Wang Y and Lee K (2018) Three-dimensional printable origami twisted tower: design, fabrication, and robot embodiment. *IEEE Robotics and Automation Letters* 3(1): 116–123.
- McCool J (2012) *Using the Weibull Distribution: Reliability, Modeling, and Inference*. Hoboken: John Wiley & Sons.
- Miron G and Plante J-S (2016) Design principles for improved fatigue life of high-strain pneumatic artificial muscles. *Soft Robotics* 3(4): 177–185.
- Miyashita S, Guitron S, Yoshida K, et al. (2016) Ingestible, controllable, and degradable origami robot for patching stomach wounds. In: Kragic D, Bichi A and De Luca A (eds) *2016 IEEE international conference on robotics and automation (ICRA)*, Stockholm, Sweden, 16–21 May 2016, pp.909–916. New York: IEEE.
- Myshkin NK, Petrokovets MI and Kovalev AV (2005) Tribology of polymers: Adhesion, friction, wear, and mass-transfer. *Tribology International* 38(11–12): 910–921.
- Nelson WB (2009) *Accelerated Testing: Statistical Models, Test Plans, and Data Analysis*. Hoboken: John Wiley & Sons.
- Nilsson M, Ingvast J, Wikander J, et al. (2012) The Soft Extra Muscle system for improving the grasping capability in neurological rehabilitation. In: *2012 IEEE EMBS conference on biomedical engineering and sciences (IECBES)*, Langkawi, Malaysia, 17–19 December, pp.412–417. 2012, New York: IEEE.
- Nycz CJ, Bützer T, Lamercy O, et al. (2016) Design and characterization of a lightweight and fully portable remote actuation system for use with a hand exoskeleton. *IEEE Robotics and Automation Letters* 1(2): 976–983.
- Odhner LU and Dollar AM (2012) The smooth curvature model: An efficient representation of Euler–Bernoulli flexures as robot joints. *IEEE Transactions on Robotics* 28(4): 761–772.
- Palli G and Melchiorri C (2006) Model, and control of tendon-sheath transmission systems. In: Normal Caplan and George Lee CS (eds) *2006 IEEE international conference on robotics and automation (ICRA)*, Orlando, FL, USA, 15–19 May 2006, pp.988–993. New York: IEEE.
- Park D and Cho K-J (2017) Development and evaluation of a soft wearable weight support device for reducing muscle fatigue on shoulder. *PLOS ONE* 12(3): e0173730.
- Pecht M (ed.) (2009) *Product Reliability, Maintainability, and Supportability Handbook, Second Edition*. 2nd edition. Boca Raton: CRC Press.
- Popov D, Gaponov I and Ryu JH (2017) Portable exoskeleton glove with soft structure for hand assistance in activities of daily living. *IEEE/ASME Transactions on Mechatronics* 22(2): 865–875.
- Sardesai AN, Segel XM, Baumholtz MN, et al. (2018) Design and characterization of edible soft robotic candy actuators. *MRS Advances* 3(50): 3003–3009.
- Shirafuji S, Ikemoto S and Hosoda K (2014) Development of a tendon-driven robotic finger for an anthropomorphic robotic hand. *The International Journal of Robotics Research* 33(5): 677–693.
- Sun Y, Song YS and Paik J (2013) Characterization of silicone rubber based soft pneumatic actuators. In: Sugano S and Kaneko M (eds) *2013 IEEE/RSJ international conference on intelligent robots and systems*, Tokyo, Japan, 3–8 November 2013, pp.4446–4453.
- Terry S, Brancart J, Lefeber D, et al. (2017) Self-healing soft pneumatic robots. *Science Robotics* 2(9): ean4268.
- Tumer IY and Stone RB (2003) Mapping function to failure mode during component development. *Research in Engineering Design* 14(1): 25–33.

- Usman M, Seong H, Suthar B, et al. (2017) A study on life cycle of twisted string actuators: Preliminary results. In: Zhang H and Vaughan R (eds) *2017 IEEE/RSJ international conference on intelligent robots and systems (IROS)*, Vancouver, Canada, 24–28 September 2017, pp.4680–4685. New York: IEEE.
- Veneman JF, Ekkelenkamp R, Kruidhof R, et al. (2006) A series elastic- and Bowden-cable-based actuation system for use as torque actuator in exoskeleton-type robots. *The International Journal of Robotics Research* 25(3): 261–281.
- Walker ID (2013) Continuous backbone “continuum” robot manipulators. *International Scholarly Research Notices* 2013. pp.1–19.
- Walker S, Rueben J, Volkenburg TV, et al. (2017) Using an environmentally benign and degradable elastomer in soft robotics. *International Journal of Intelligent Robotics and Applications* 1(2): 124–142.
- Wang Z, Torigoe Y and Hirai S (2017) A prestressed soft gripper: design, modeling, fabrication, and tests for food handling. *IEEE Robotics and Automation Letters* 2(4): 1909–1916.
- Wehner T and Fatemi A (1991) Effects of mean stress on fatigue behaviour of a hardened carbon steel. *International Journal of Fatigue* 13(3): 241–248.
- Witte KA, Zhang J, Jackson RW, et al. (2015) Design of two lightweight, high-bandwidth torque-controlled ankle exoskeletons. In: *2015 IEEE international conference on robotics and automation (ICRA)*, Seattle, USA, 26–30 May 2015, pp.1223–1228. New York: IEEE.
- Yang Z and Lin DKJ (2007) Improved maximum-likelihood estimation for the common shape parameter of several Weibull populations. *Applied Stochastic Models in Business and Industry* 23(5): 373–383.
- Yap HK, Lim JH, Nasrallah F, et al. (2015) A soft exoskeleton for hand assistive and rehabilitation application using pneumatic actuators with variable stiffness. In: Parker L and Amato N (eds) *2015 IEEE international conference on robotics and automation (ICRA)*, Seattle, USA, 26–30 May 2015, pp.4967–4972. New York: IEEE.
- Yap HK, Ng HY and Yeow C-H (2016) High-force soft printable pneumatics for soft robotic applications. *Soft Robotics* 3(3): 144–158.
- Zhu S-P, Lei Q, Huang H-Z, et al. (2017) Mean stress effect correction in strain energy-based fatigue life prediction of metals. *International Journal of Damage Mechanics* 26(8): 1219–1241.